Radiation tests of FCA device for HENON mission

Laboratory of Cyclotron and Fast Neutron Generators

Zdenek Nemecek

Proposal ID

619

Conclusion

The FCA device was irradiated with 32,54 MeV proton beam and the current in the range from 8,00E-10A to 2,20E-07A (see the table).

FC0 was facing toward the proton beam (Figure 6) its open entrance window, window of FC1 was closed. Both collectors of FC0 were connected to corresponding amplifiers whereas the FC1b collector was disconnected in order to monitor effects of radiation on the amplifier itself. The suppressor grid voltages were adjusted to 300 V, the control voltage was sweeping from 100 to 1200 V with the period of 6 s.

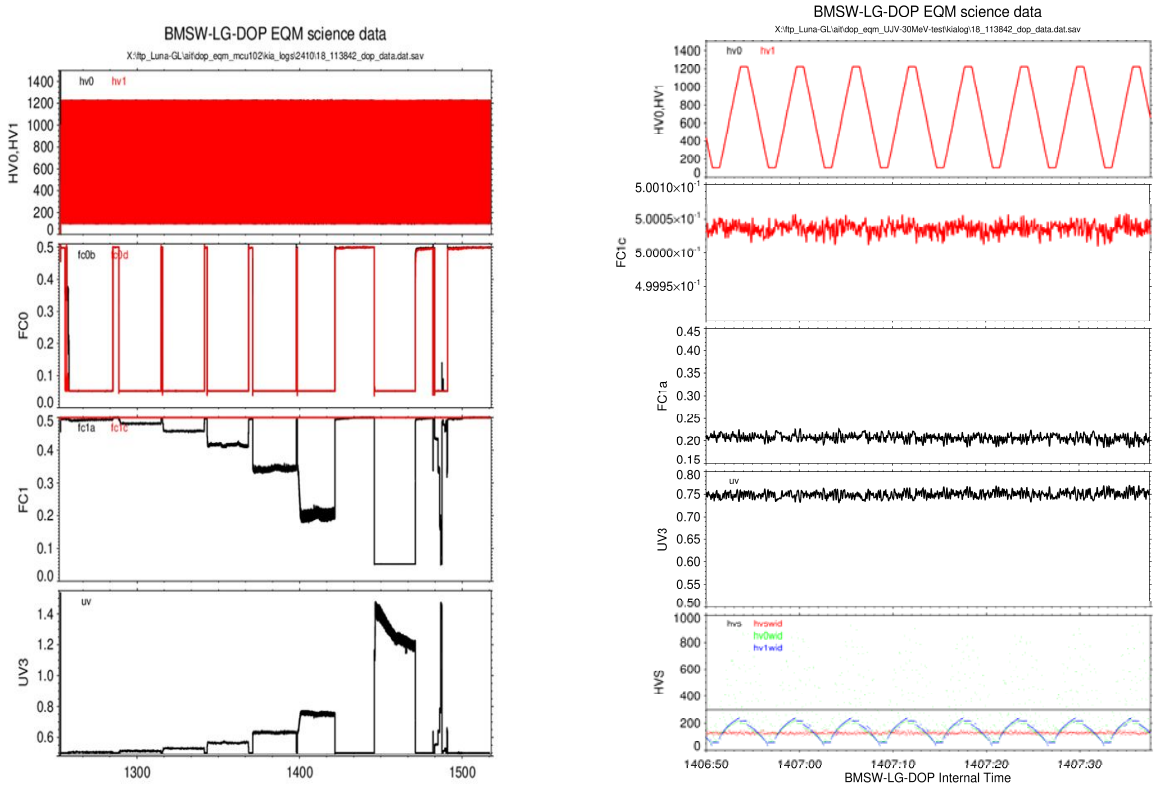

Figure 9. Left – Record of (from to bottom) control grid voltages, FC0 currents, FC1 currents, current recorded by UV detector. Right - (from to bottom) output of monitors of control grid voltages, output of FC1c amplifier, output of FC1c amplifier, output of UV detector, system monitors of HV sources.

Left part of Figure 9 demonstrates that there was no reset or any other interruption of the tests. Amplifiers of both collectors of FC0 cup are saturated by products of ionization inside the cup and secondary electrons generated by proton impacts. The FC1a amplifier measures current that is roughly proportional to the beam current (it is saturated by the highest beam current), the disconnected FC1c amplifiers does not register any current. The amplifier of UV detector (not used in FCA) registers current that is proportional to the proton beam current.

Right part of the figure shows a blow-up of about 50 seconds of measurements. The noise of the disconnected FC1c amplifier is enhanced to about 20μV_{pp} due to impacts of energetic protons, FC1a and UV3 measure the noise connected with variations of ionization products. The system monitors of HV amplifies do not exhibit any malfunction.

We can conclude that BMSW-LG-DOP passed the test successfully.

Calibration and Performance Testing of the NCAL Detector System by Cyclotron-Generated Neutron Beams

Laboratory of Cyclotron and Fast Neutron Generators

Vladimír Wagner

Proposal ID

638

Report regarding proposal " Calibration and Performance Testing of the NCAL Detector System"

Petr Chaloupka[1], Otari Javakhishvili[1], Andrej Kugler[2], Vladimír Wagner[2], Dieter Grzonka[3] and Dachi Okropiridze[3]

[1] Czech Tech. Uni. in Prague, FNSPE, Czech Republic [2] Nucl. Physics Inst., Řež, Czech Republic
[3] Bochum University, Germany

In heavy-ion collisions at the Compressed Baryonic Matter (CBM) experiment [1], detecting projectile spectators is crucial for characterizing the reaction. The CTU and NPI Řež lead a development of a new Forward Spectator Detector (FSD) for CBM based on a scintillator hodoscope design. The proposed FSD will have similar functionality as the Forward Wall detector of HADES experiment, which was previously designed and delivered by NPI Řež. The detector will be capable of detecting charged particles from collisions at rates of up to 10 MHz. However, such a detector would not be able to detect spectator neutrons, which also carry valuable information. To address this, it was proposed to include modules of the NCAL (neutron calorimeter). The performance of these modules for neutron detection is currently under investigation. The NCAL detector is being developed in collaboration with Bochum University, NPI Řež, and CTU.

The NCAL consists of hexagonal BC-416 plastic scintillator modules arranged in a honeycomb pattern, each coupled to XP4592/PA photomultiplier tubes (PMTs). The modules were originally designed for charged particle detection in COSY-TOF spectrometer. The scintillators detect neutrons through elastic scattering, where recoiling protons generate scintillation light. The primary goal of this project is to validate and calibrate the response of the NCAL modules to neutrons. The focus is on achieving precise energy calibration, characterizing neutron detection efficiency, and validating custom DAQ systems in a controlled environment. This includes measuring absolute detection efficiency and calibrating the energy response.

To achieve this, a neutron field through the p + Li reaction at proton beam energy of 32.5MeV was generated. The challenge of the experimental setup was to actually achieve low enough intensities so that there is at maximum only one neutron per spill impinging on the detector. The detector was placed at the maximum possible distance of 4.3 m from the target. Given the beam intensity in the range from 0.1 to 5μA, it is expected that the neutron flux at the target should be $\sim 10^3$–10^4cm^{-2}s^{-1}. In order to be able to perform absolute calibration and to characterize the detector response, the detector was read out in parallel by an oscilloscope (saving full waveforms for selected runs) and via DiRICH system. The DiRICH is a novel DAQ system with triggerless readout for very high event rates developed at GSI [2, 3]. Reference RF signal from cyclotron (25 MHz) was used for triggering.

References

[1] V. Friese. The cbm experiment at gsi/fair. *Nuclear Physics A*, 774(1–4):377–386, 2006.

[2] V. Friese. Event reconstruction in the tracking system of the cbm experiment. *EPJ Web of Conferences*, 226:01004, 2020.

[3] T. Becker et al. Qualification of dirich readout chain. *Nuclear Instruments and Methods in Physics Research Section A: Accelerators, Spectrometers, Detectors and Associated Equipment*, 1056:168570, 2023.

Two-dimensional waveguides in glass created by multi-energetic ion implantation via photoresist mask

Laboratory of Tandetron

Romana Mikšová

Proposal ID

575

Report regarding proposal "Two-dimensional waveguides in glass created by multi-energetic ion implantation via photoresist mask"

Romana Mikšová [1]*, Pavla Nekvindová[2], Petr Aubrecht[3], Anna Macková[1,4]

[1]*Nuclear Physics Institute CAS, Hlavní 130, 250 68 Rez, Czech Republic*
[2]*Department of Inorganic Chemistry, University of Chemistry and Technology in Prague, 166 28 Prague, Czech Republic*
[3]*Centre for Nanomaterials and Biotechnology, Faculty of Science, Jan Evangelista Purkyně University in Ústí nad Labem, 400 96 Ústí nad Labem, Czech Republic*
[4]*Department of Physics, Faculty of Science, University of J. E. Purkyně, Pasterouva 3544/1, 400 96 Ústí nad Labem, Czech Republic*

In the presented study the fabrication of optical waveguides in various silicate glasses (S-1, Gil11, BK7) using the single and multi-energy implantation of C^+ ions via photoresist mask (Fig. (a) and (b)). The elemental composition of pristine glasses and photoresist mask was determined using RBS method with 2 MeV He ion before implantation (Fig. (c)). These parameters were used for precise simulation of projected range in glasses.

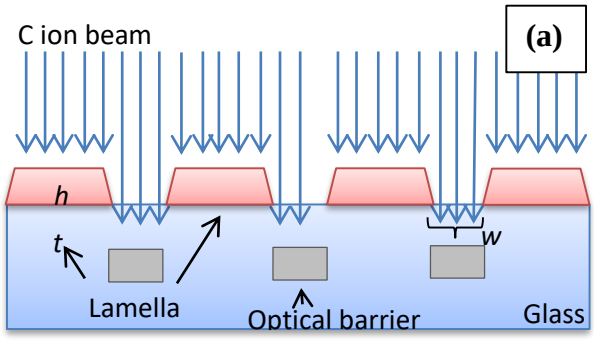

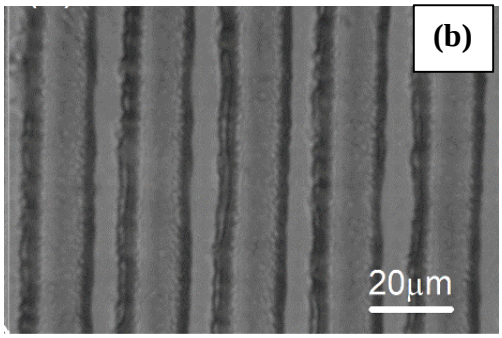

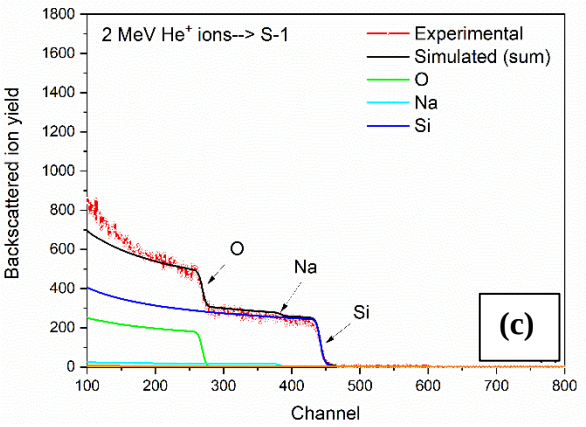

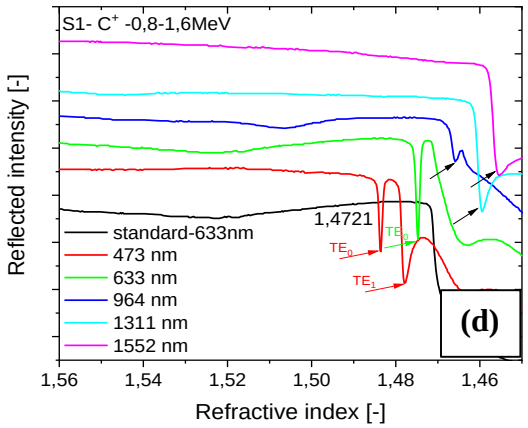

The optical modes are significant in S-1 glass where the range of the carbon ions is expected to be the deepest and hence the layer is the widest. Also obvious is the difference between multi and single-energy implantation, where at 473 nm only one mode of light propagates for single C ions implantation and two modes for sequential implantation (Fig. (d)). In the other two types of glass (GIL11 and BK7) either less or no number of modes is seen even at low wavelengths. This trend corresponds very well with the predicted depth of carbon projected range and takes with the indicated difference between multi and single-energy implantation. The properties of the glass substrate were in line with our assumptions. The glass S-1 with the highest content of silicate network showed the lowest density, and the glass BK7 containing Ba^{2+} ions as a modifier showed the highest density.

The results will be presented at European conference on applications of surface and interface analysis 2024 and published in Surface and Interface Analysis proceedings in the July of 2024.

Diffusion of oxygen into a polymer-like film

Laboratory of Tandetron

Vladimir Cech

Proposal ID

595

Report on the proposal “Diffusion of oxygen into a polymer-like film”

Vladimir Cech, Brno University of Technology, Brno, Czech Republic
Oleksandr Romanenko, Anna Macková, Nuclear Physics Institute, Rez, Czech Republic

Nonthermal plasma-deposited sandwich structures consisting of glassy silica and a polymer layer in various orders were covered with an ultrathin barrier coating of silicon carbide to prevent the diffusion of atmospheric oxygen and water molecules into the polymer material.

Fresh and aged sandwich structures (Fig. 1) were analyzed using RBS / ERDA techniques to determine the possible oxidation of the polymer material. The simulated data required the addition of a thin interlayer between the oxide and polymer layers at the expense of the polymer layer thickness to fit the experimental data (Fig. 2).

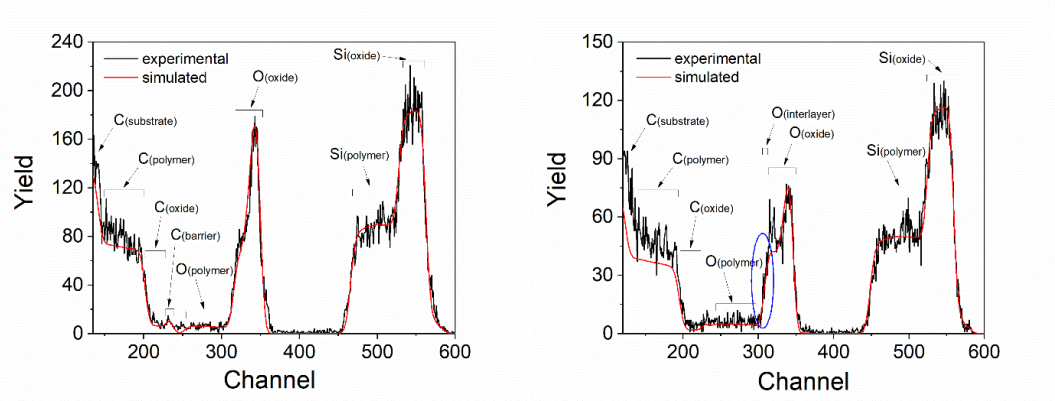

Fig. 1. RBS spectra of (a) 45 days and (b) 831 days stored sandwich structure.

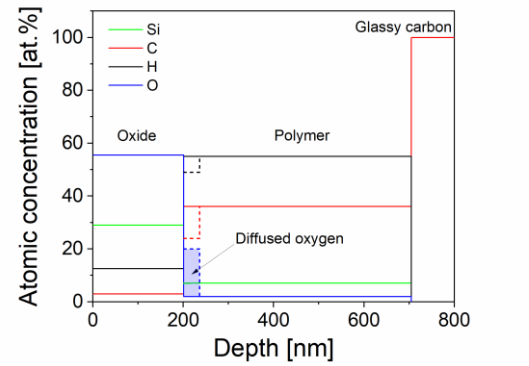

Fig. 2. Elemental depth profile of as-deposited (solid line) and aged (dashed line) sandwich structure. Diffused oxygen is indicated by the blue area.

This study revealed that glassy silica is a slightly porous material (3 vol.%) with small pores (2.5 nm) formed during thin film deposition and containing gaseous carbon dioxide. These CO_2 molecules can diffuse from the silica layer through the silicon oxide/polymer interface into the polymer material. The low-cross-linked polymer material is then oxidized because of complex chemical reactions that change its chemical and physical properties. This means that the silicon oxide/polymer interface gradually moves into the polymer material over time (Fig. 3). The diffusion coefficient of CO_2 in the polymer estimated to be 4.4×10^{-25} m^2 s^{-1} resulted in a shift of the silicon oxide/polymer interface of 35 nm after 27 months.

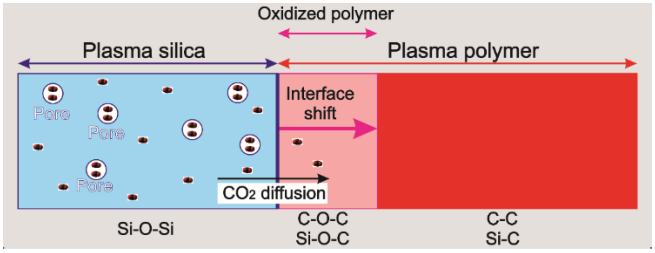

Fig. 3. Schematic view of CO_2 diffusion from glassy silica into a polymer material.

Controlled fabrication of self-assembled iron-fullerene nanocomposite films

Laboratory of Tandetron

Vasyl Lavrentiev

Proposal ID

582

Project title: **Controlled fabrication of self-assembled iron-fullerene nanocomposite films**

Researcher: **Vasily Lavrentiev**

Affiliation: *Nuclear Physics Institute CAS, Rez-130, Husinec, 250 68*

Project term: *1.4.2023-1.1.2024* (proposal 582)

By implementing this cycle of the experiments, the goal of the project was achieved, namely, (1) the obtained results evidence successful creation of the Fe-C_{60} nanocomposite (NC) films through self-assembly phenomenon, and secondly, (2) stability of the Fe-C_{60} structure and composition upon keeping the films in an ambient air was verified. The required information has been obtained using Rutherford backscattering spectrometry (RBS) and atomic force microscopy (AFM) techniques. The Fe-C_{60} NC films have been fabricated through simultaneous deposition of Fe and C_{60} on Si(100) using physical vapor deposition technique. 1). According to our previous results, the applied deposition setup should lead to formation of nanocomposite nanostructure as a uniform ensemble of the Fe nanoparticles (NPs) immersed in the C_{60} medium [1, 2]. Formation of such a specific nanostructure is confirmed by analysis of the RBS spectra, some of which are shown in *Figure 1a*. Except the anticipated Fe and C components, the RBS spectra also include the ion scattering effect from oxygen at the deposited layers, which, evidently, was introduced during the sample transfer to the RBS chamber (the ion-beam experiments are in *ex-situ* conditions). Analysis of the correlations between the Fe and O contents in the deposited samples implies the formation of the oxidized Fe NPs [1]. 2). *Figure 1b* demonstrates the RBS spectra recorded from the $Fe_xO_yC_{60}$ films with $x \approx 12$ recorded from the samples kept at the ambient air during different time. The RBS spectra show only slight change revealing some increase in the O content at the longer air exposure. At the same time, AFM does not distinguish serious changes in the surface topography after the air exposure (see *Figure 1c*).

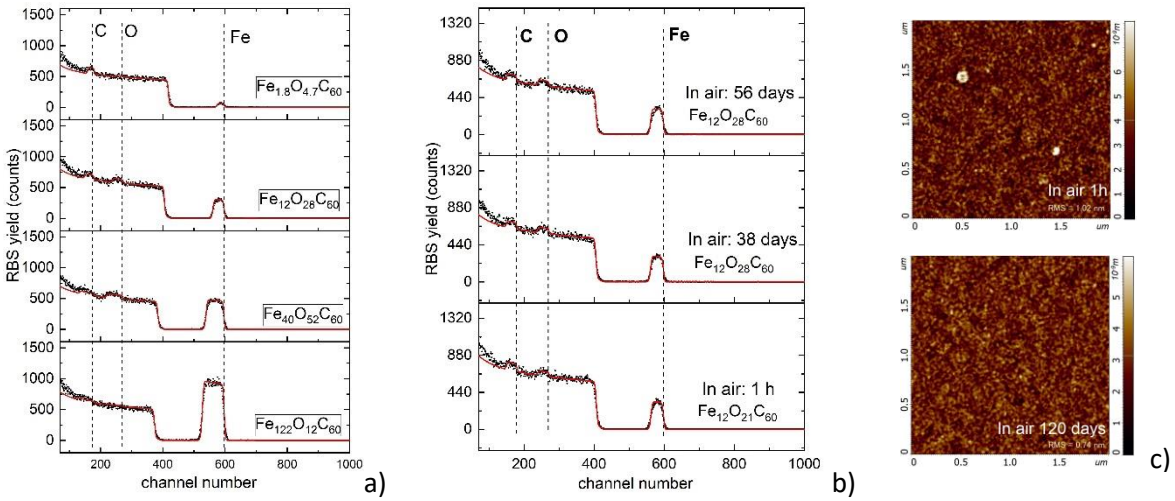

Figure 1. **(a)** The experimental (black dots) and simulated (red lines) RBS spectra of the as-deposited $Fe_x(O_y)C_{60}$ films with different Fe content. **(b)** The RBS spectra of the $Fe_x(O_y)C_{60}$ film with $x \approx 12$ recorded after the different times of the sample air exposure. **(c)** AFM images of the surface of the film with $x=12$ as-deposited (top image) and after the air exposure for 120 days (bottom image).

The results obtained within this project will be published soon in some international journals.

References

1. V. Lavrentiev et al. Carbon 103 (2016) 425.
2. V. Lavrentiev et al. Carbon 184 (2021) 34.

Radiation hardness study of diamond based detector structures

Laboratory of Tandetron

Bohumír Za?ko

Proposal ID

630

Report of the proposal: Radiation hardness study of diamond based detector structures

Diamond based detector structures were irradiated by 4 MeV protons with four different fluences 1×10^{13} cm^{-2}, 1×10^{14} cm^{-2}, 1×10^{15} cm^{-2}, 1×10^{16} cm^{-2}, respectively. Irradiated structures were analyzed using positron annihilation spectroscopy. Positrons annihilate mainly in the diamond layer (estimated at around 80%). The remaining 20% reach the Si substrate, which to some extent affects the overall results. The mean lifetime of positrons should increase with a total fluence of 4 MeV protons, but this was not confirmed by measurements. The figure1 on the left shows a decreasing dependence of the mean lifetime with increasing proton fluence. The lifetime decreases from a value of 246ps for the unirradiated sample to a value of 238ps for the highest fluence. A certain deviation to a monotonic dependence was observed at a fluence of 10^{15} cm^{-2}, but the explanation of this discrepancy will require a more detailed analysis. The overall decreasing dependence indicates a high concentration of defects (vacancies) in the original layer and proton irradiation reduces the effective lifetime of positrons. The $\tau2$ component (figure on the right) – the short defect component grows with fluence from a value of 208ps to a value of about 238ps, which corresponds to the growth of vacancy clusters. Thus, irradiation does not create new clusters, but rather enlarges existing ones.

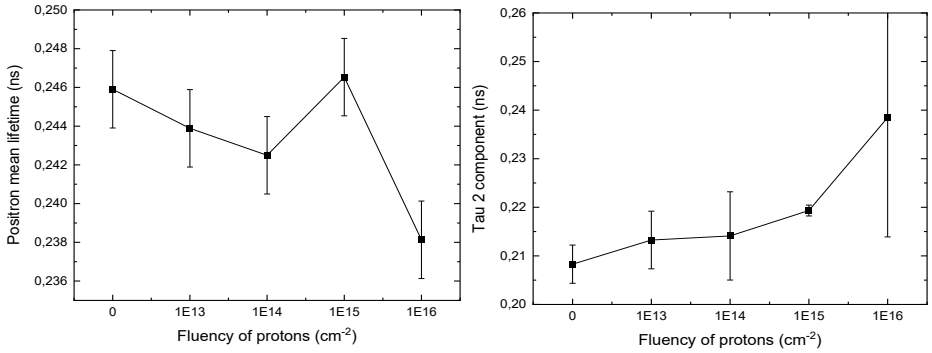

Fig. 1: Mean lifetime of positrons in irradiated diamond samples as a function of the fluence of 4 MeV protons (left); dependence of the $\tau2$ component on fluence (right).

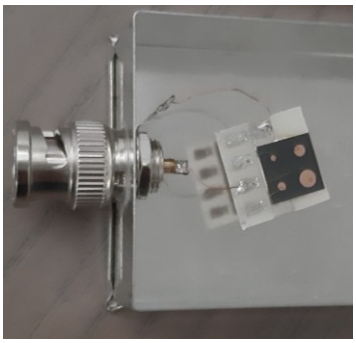

Fig. 2: Detection structures based on polycrystalline diamond prepared for spectrometric measurements.

Subsequently, circular contacts with diameters from 1 to 3 mm were prepared on the diamond side by depositing Au in a high vacuum apparatus. Figure 2 shows the glued diamond structure on the support, contacted, placed in a box with a BNC connector and prepared for spectrometric measurements. For testing, we used a standard spectrometric path consisting of a charge-sensitive preamplifier and a CAEN HEXAGON digital amplifier. As a radiation source, we used 5.5 MeV α-particles generated by the radioisotope ^{241}Am.
Figure 3 shows a comparison of detection α-particle spectra for non-irradiated and proton-irradiated diamond layers with different sizes of prepared contacts. The measured spectra show a gradual degradation of the diamond layers (shift of the detection peak to lower channels) with increasing proton fluence. In the case of samples with a contact diameter of up to 1.5 mm, the detection peak is distinguishable from noise even at a fluence of 10^{14} p/cm^2, however, for a larger contact (2 mm) it is already at the noise limit of the spectrometric path. This is due to the fact that the peak position before irradiation is at about 50% of the level of samples with smaller contacts. In conclusion, it can be said that during the degradation of diamond layers by protons, the detection peak shifts towards lower channels, which means a decrease in the amplitude of the pulses generated during the detection of alpha radiation. Since the amplitude of the detected pulses also decreases with the increasing area of the prepared contact, samples with a larger contact are able to operate only up to lower irradiation fluences.

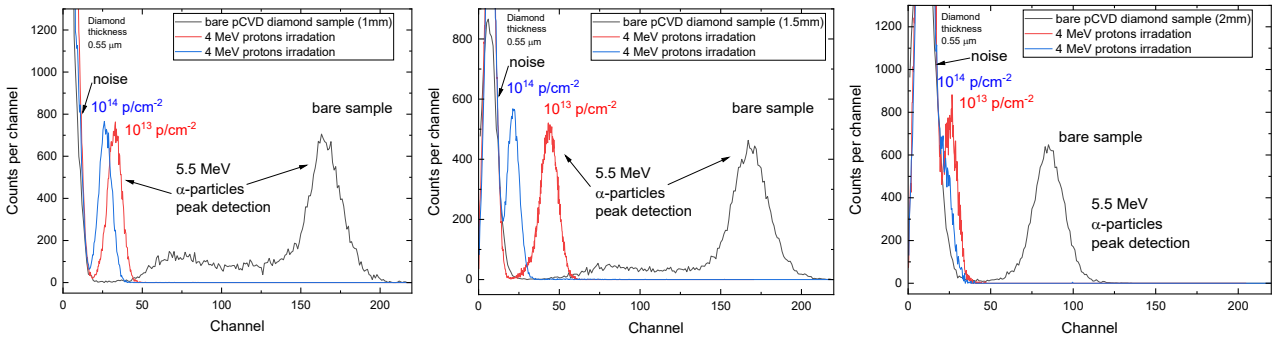

Fig. 3: Detection spectra of α-particles using diamond detectors with a different size of Au contacts (1; 1.5 and 2 mm) before and after proton irradiation with fluences of 10^{13} p/cm^2 a 10^{14} p/cm^2.

Residual stresses analysis by neutron diffraction in duplex stainless steel samples produced by AM

Neutron Physics Laboratory - Neutron diffraction

Massimo Rogante

Proposal ID

631

Neutron diffraction analysis of duplex stainless steel samples produced by AM (Exp. NPL631 at SPN-100)

M. Rogante [(1)], F. Fiori [(2)]
(1) Rogante Engineering Office, Civitanova Marche, Italy
(2) Università Politecnica delle Marche, Ancona, Italy

Tab. I. Investigated samples.

Sample	Laser power [W]	Scan speed [mm/s]	Hatch spacing [mm]	Layer thickness [mm]	Density
1.1	250	600	0,14	0,05	98.6%
1.2		800	0,14	0,05	98.2%
1.3		1000	0,14	0,05	96.1%
1.4	230	600	0,14	0,05	98.9%
1.5		800	0,14	0,05	97.8%
1.6		1000	0,14	0,05	95.4%

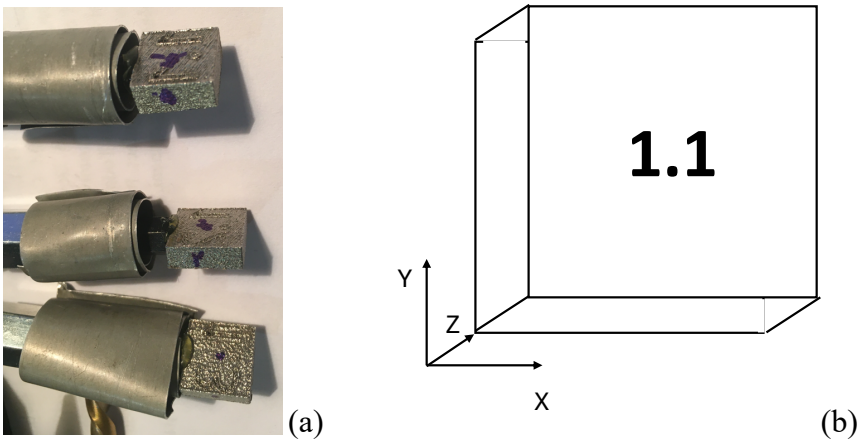

(a) (b)

Fig. 1. (a) Investigated samples, mounted on sample holders; (b) definition of principal directions X, Y, Z.

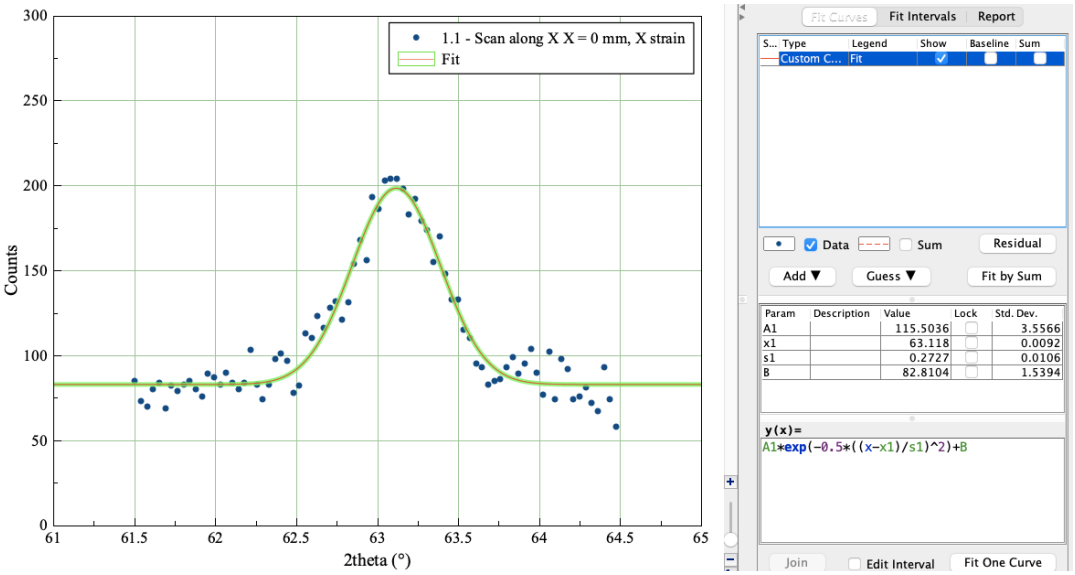

Fig. 2. Example of the Bragg peaks obtained, showing that only the bcc phase is present.

Modification of graphene and polymer thin films by multi-energy implantation of Cu and Ag ions

Laboratory of Tandetron

Eva Štpanovská

Proposal ID

600

Final report proposal: Modification of graphene and polymer thin films by multi-energy implantation of Cu^+ and Ag^+ ions

As part of the experiments, multi-energy implantation of Cu^+ and Ag^+ ions was performed into multilayer graphene and polymeric materials (PI, PMMA, COC) to modify their properties for potential application in lithium-ion batteries (LIBs).

For graphene, the implantation aimed to mitigate restacking, which reduces active surface area and degrades electrochemical stability. The gradient distribution of metal ions was designed to create electrostatic pillars that maintain layer separation and enable efficient lithium-ion transport. **Figure 1 presents the Raman spectra of graphene after Cu^+ implantation, showing an increase in sp^2 bond intensity and the 2D peak, indicating preserved conductivity while modifying interlayer interactions.**

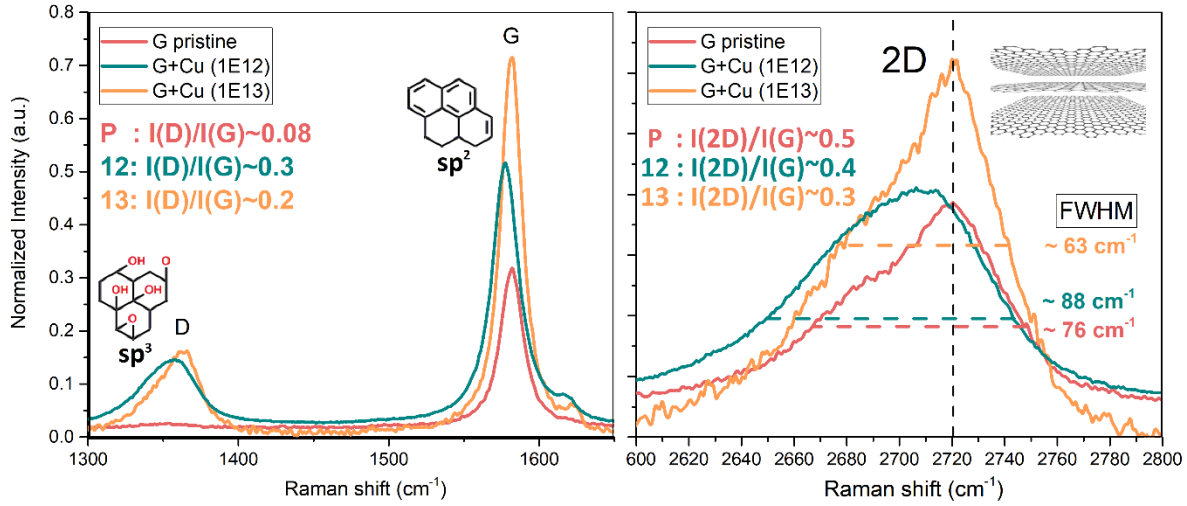

Figure 1 Raman spectra of multilayer graphene before and after Cu^+ ion implantation at fluences of 1×10^{12} cm^{-2} and 1×10^{13} cm^{-2}. The increase in the D band intensity (I(D)/I(G)) indicates defect formation, while the 2D band remains prominent, suggesting preserved sp^2 domains. The narrowing of the 2D peak (FWHM) with fluence suggests modifications in interlayer interactions, potentially reducing restacking effects.

For polymers, implantation focused on enhancing dielectric and mechanical properties. PI was modified to improve polarizability and adhesion, PMMA to enhance ionic conductivity through interactions between implanted ions and carbonyl groups, and COC was investigated as a potential protective layer for SEI stabilization. The multi-energy approach ensured a gradual modification from the surface to the bulk, with low fluences inducing minor structural changes and higher fluences promoting conductive pathways and polymer cross-linking.

[1] Adenusi, H., et al. (2023). Lithium Batteries and the Solid Electrolyte Interphase (SEI)—Progress and Outlook. In Advanced Energy Materials (Vol. 13, Issue 10). Wiley.
[2] An, S. J., et al. (2016). The state of understanding of the lithium-ion-battery graphite solid electrolyte interphase (SEI) and its relationship to formation cycling. In Carbon
[3] Shen, Y., et al. (2021). Achieving Desirable Initial Coulombic Efficiencies and Full Capacity Utilization of Li?Ion Batteries by Chemical Prelithiation of Graphite Anode.

Neutron diffraction analysis of duplex stainless steel samples produced by AM

Neutron Physics Laboratory - Neutron diffraction

Massimo Rogante

Proposal ID

632

Tab. I. Investigated samples.

Sample	Laser power [W]	Scan speed [mm/s]	Hatch spacing [mm]	Layer thickness [mm]	Density
1.1	250	600	0.14	0.05	98.6%
1.2		800	0.14	0.05	98.2%
1.3		1000	0.14	0.05	96.1%
1.4	230	600	0.14	0.05	98.9%
1.5		800	0.14	0.05	97.8%
1.6		1000	0.14	0.05	95.4%

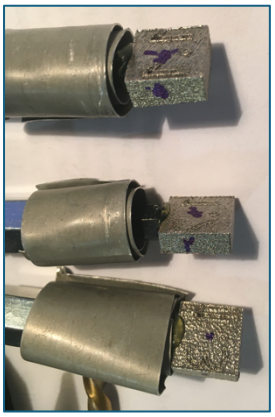

Fig. 1. Three of the investigated samples, mounted on sample holders.

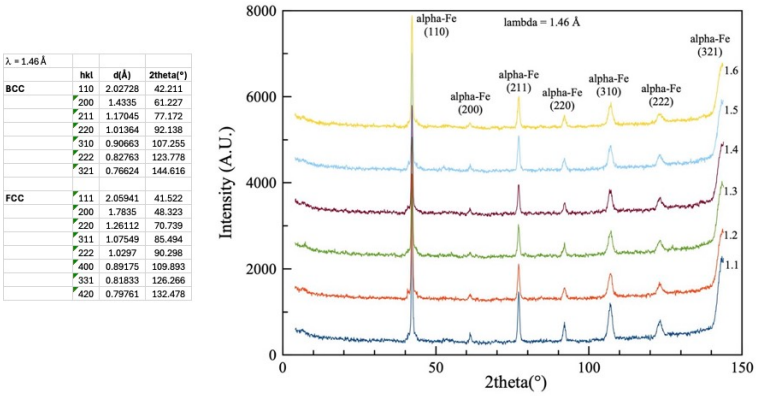

λ = 1.46 Å

	hkl	d(Å)	2theta(°)
BCC	110	2.02728	42.211
	200	1.4335	61.227
	211	1.17045	77.172
	220	1.01364	92.138
	310	0.90663	107.255
	222	0.82763	123.778
	321	0.76624	144.616
FCC	111	2.05941	41.522
	200	1.7835	48.323
	220	1.26112	70.739
	311	1.07549	85.494
	222	1.0297	90.298
	400	0.89175	109.893
	331	0.81833	126.266
	420	0.79761	132.478

Fig. 2. Measured diffraction patterns.

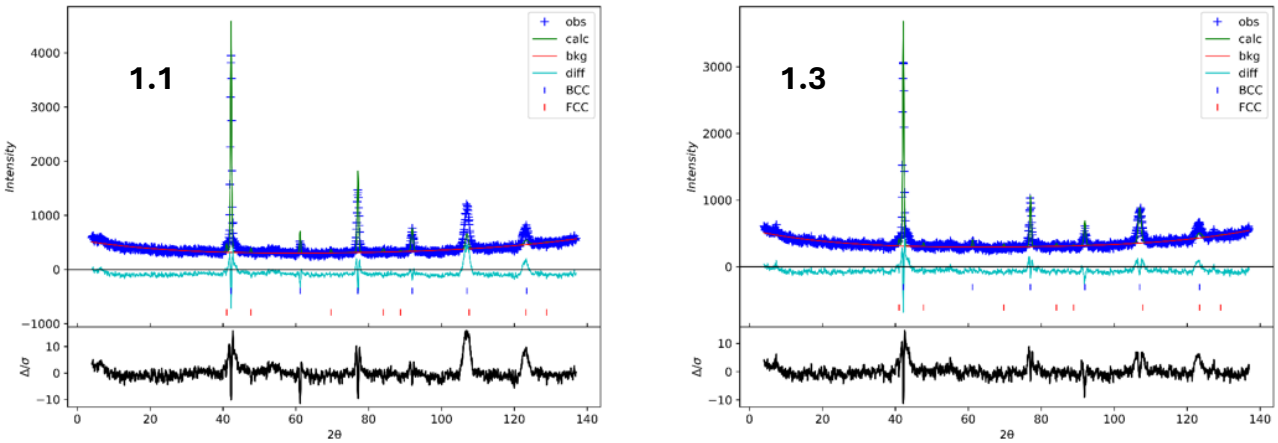

Fig. 3. Rietveld refinements for samples 1.1 and 1.3.

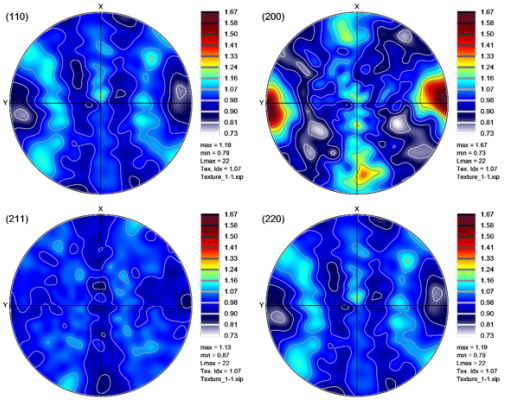

Fig.4. Pole figures for sample 1.1.

Gaining insights into the nanostructure–properties relationship of Ionic Liquids/Polymer composites

Neutron Physics Laboratory - Neutron diffraction

Vera Macedo

Proposal ID

633

Experiment Report (Ultra Small Angle Neutron Scattering – Proposal **NPL_633**) "Gaining insights into the nanostructure – properties relationship of Ionic Liquids/Polymer based composites"

The study aims to analyse the influence of different fillers on the matrix physicochemical properties as well as the battery performance of these composites as solid electrolytes. In addition to the analysis to obtain the former properties information - FTIR, DSC, TGA, EIS, and among others -, was also performed a study at the nanostructure level with small angle neutron scattering (SANS). Although, an inhomogeneities at low Q values was identified in one of the samples, thus surging the urge of measure ultra-small angle scattering, in order to analysis the nanostructure at that scattering length. Despite the fact of only being detected the uncommon inhomogeneity on only one sample, there were analysis with U-SANS all 7 composites samples to confirm such structure in the rest. The composites consist of a PVDF-HFP matrix with addition of several fillers such as ionic liquid ([BMIM][SCN]), lithium salt (LiTFSI) and zeolite (clinoptiolite). As the strange inhomogeneity appears to Q<0.01 $\dot{A}$, the U-SANS measure was performed not only low (~ 0.002-0.02 $\dot{A}$) and medium resolution (~ 0.0005-0.002 $\dot{A}$) but also at high resolution (~ 0.0002-0.005) to be able to analyse the tendency of the curve. As observed in Figure1., the presence of the inhomogeneity at low Q values was confirmed with U-SANS (red curve from Figure1.b) and c)), detected at medium resolution 0.001>Q<0.01, not being observed in the others as expected. This outcome has great important to the study, since highlight the major interference of ionic liquids not only on the physicochemical and battery performance, but also on the nanostructure of PVDF.

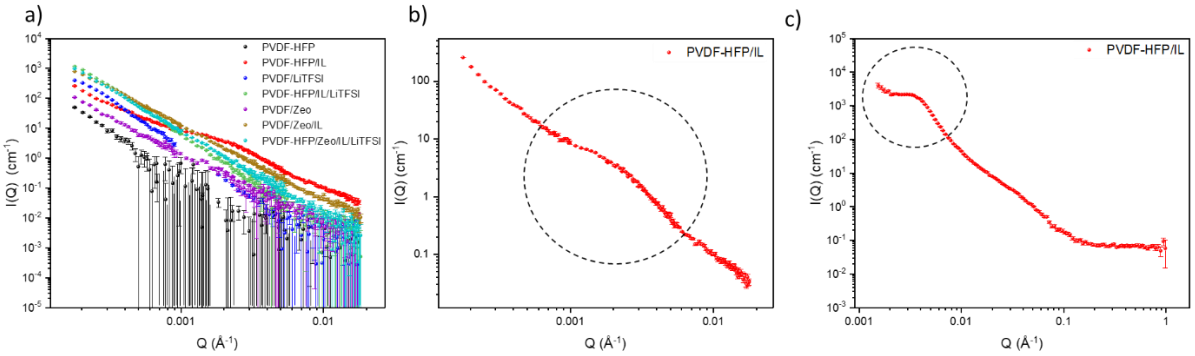

Figure 1. a) U-SANS data of all measured samples and b) U-SANS and c) SANS of PVDF-HFP/IL sample.

The next step will involve a more detailed analysis of the obtained data, correlating it with the other results to incorporate it into the article manuscript.

USANS Contrast Variation Analysis of Equilibrium Aggregates in Concentrated Aqueous Ferrofluids

Neutron Physics Laboratory - Neutron diffraction

Anatolii Nagornyi

Proposal ID

618

Report regarding proposal “USANS Contrast Variation Analysis of Equilibrium Aggregates in Concentrated Aqueous Ferrofluids”

A.Nagornyi. *CERIC-ERIC, Basovizza, Italy*
O.Tomchuk. *ISIS, Didcot, Great Britan*
V.Socoliuc. *Center for Fundamental and Advanced Technical Research, Timisoara, Romania*

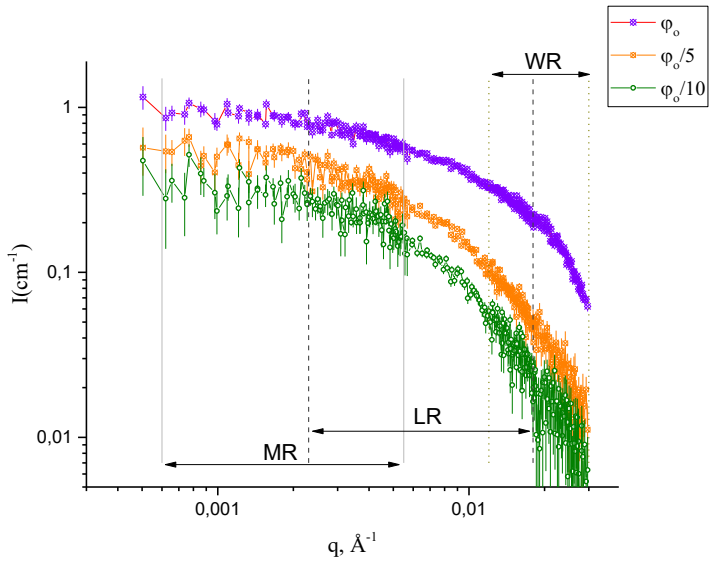

Fig. 1. Small-angle neutron scattering curves: reduction of magnetic material concentration by a factor of 5 and 10 through dilution with light water.

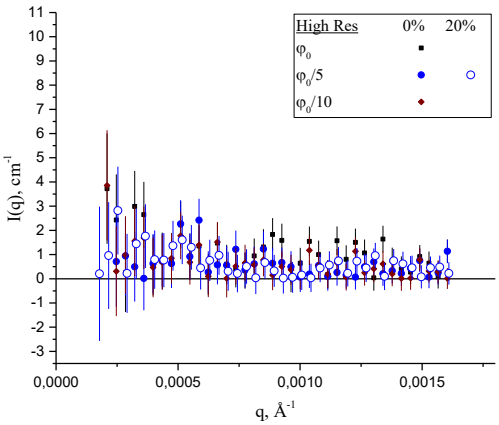

Fig. 2. Typical dependencies in the highest "Q" value interval, high-resolution mode. Three concentrations of magnetic fluid in light water, including an addition of 20 vol.% heavy water, are presented.

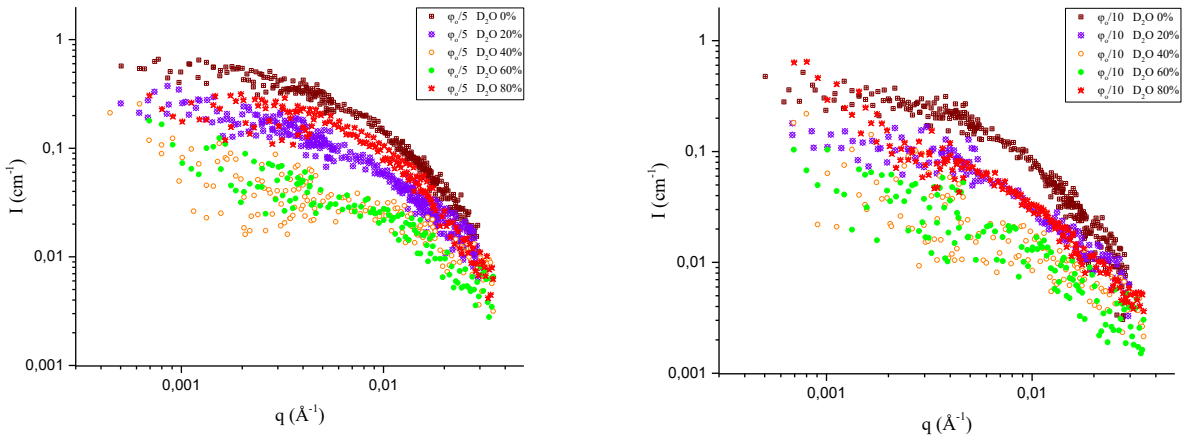

Fig. 3. Variation of neutron contrast in magnetic fluid at two concentrations, φ₀/5 and φ₀/10: dilution was performed to achieve heavy water volume fractions of 20, 40, 60, and 80%